ADVANCED THEORY AND SIMULATIONS
www.advtheorysimul.com

First-Principles Study of the Stability, Physical Properties, and Molecular Dynamics in $KSrZH_6$ (Z = Rh, Ir) for Hydrogen Storage Applications

Aya Chelh, Boutaina akenoun, Smahane Dahbi, Hamid Ez-Zahraouy, E. A. Elghmaz, N.S. Abd EL-Gawaad,* Mohammed S. Abu-Jafar, and Asif Hosen**

This study examines the structural, electronic, optical, elastic, thermodynamic, and hydrogen storage properties of $KSrZH_6$ (Z = Rh, Ir) utilizing density functional theory to explore their potential as hydrogen storage materials. The structural analysis confirms that all the studied materials crystallize in the cubic phase with space group 216 ($F\bar{4}3m$). The phonon dispersion and ab initio molecular dynamics (AIMD) computations reveal dynamic and thermal stability for both compounds. In addition, the electronic structures exhibit indirect semiconducting properties, with an extensive hybridization near the Fermi level between 1s-orbitals of hydrogen (H), and d-orbitals of the transition metals (Rh and Ir). Furthermore, optical investigations reveal significant UV absorption, as well as a moderate refractive index and reflectivity, which can be useful in optoelectronic devices. All of the studied materials possess mechanical stability and show brittle properties. Among the compounds, $KSrRhH_6$ exhibits the highest gravimetric hydrogen storage capacity of 2.57 wt.%, while $KSrIrH_6$ shows a slightly lower value of 1.86 wt.%. The storage capacity decreases when the cationic atom Rh is substituted with Ir, attributed to variations in atomic radius. This comprehensive study underscores the promising potential of $KSrZH_6$ (Z = Rh, Ir) for both hydrogen storage and optoelectronic applications.

1. Introduction

Growing concerns about global warming, depletion of natural resources, and pollution have increased the need to move away from fossil fuels to other sustainable forms of energy.[1] Fossil fuels have long been the cornerstone of industrial and economic development,[2] but their negative impact on the environment, mainly through greenhouse gas emissions, has led to serious climate problems.[3,4] Hydrogen energy has gained significant attention as a promising alternative because of its abundance, superior energy density, and clean combustion, producing only water vapor.[4–7] However, despite its technical and environmental advantages, the widespread use of hydrogen energy is still hampered by the inherent difficulties of storing and transporting it, especially in ambient conditions.[8–11] Due to its improved safety, reversible storage capacity, and generally mild operating conditions, material-based hydrogen storage, especially in the form of metal hydrides, has garnered a lot of attention.[12–14] As a result, hydrogen energy has maintained a significant advantage and emerged as a key renewable resource in the pursuit of sustainable development.[15,16] Thanks to their high hydrogen concentration and reversible desorption/adsorption characteristics, complex hydrides are a broad family of materials that have been thoroughly investigated for hydrogen storage applications.[17] The systems of this class of

A. Chelh, B. akenoun, S. Dahbi, H. Ez-Zahraouy
Laboratory of Condensed Matter and Interdisciplinary Sciences
"Labeled Research Unit CNRST"
URL-CNRST-17
Faculty of Sciences
Mohammed V University in Rabat
Rabat 1014, Morocco
E-mail: aya.chelh@um5r.ac.ma

E. A. Elghmaz
Department of Physics
King Khalid University
Abha 61421, Saudi Arabia

N. A. EL-Gawaad
Health Specialties, Basic Sciences and Applications Unit
Applied College
King Khalid University
Muhayil Asir Abha 62529, Saudi Arabia
E-mail: Nshat@kku.edu.sa

M. S. Abu-Jafar
Department of Physics
An-Najah National University
Nablus 7, Palestine

A. Hosen
Department of Materials Science and Engineering
Khulna University of Engineering & Technology (KUET)
Khulna 9203, Bangladesh
E-mail: asif@mse.kuet.ac.bd

The ORCID identification number(s) for the author(s) of this article can be found under https://doi.org/10.1002/adts.202500622

DOI: 10.1002/adts.202500622

materials, including transition metal, alkali metal, and alkaline earth metal hydrides, have demonstrated significant promise in addressing the expanding demand for sustainable and clean energy. All of these compound's intrinsic qualities, such as metal-hydrogen bonding, structural stability, and thermodynamic characteristics, greatly influence their capacity to store hydrogen; as a result, choosing the best options necessitates extensive research.[18]

Theoretically, numerous complex hydrides such as Mg_2TH_y (T = Ni, Co, Fe),[19] Mg_2CoH_5,[20] $NaAlH_4$,[21] Mg_2FeH_5,[22] $NaMgH_2F$,[23] Cs_2SrTlH_6,[24] Cs_2BaTlH_6,[24] XGaSiH (X = Sr, Ca, Ba),[25] A_2BH_6 (A = K, Rb; B = Ge, Sn),[26] $KNaX_2H_6$ (X = Mg, Ca),[27] AlX_3H_9 (X = Ca, Sc, Zr),[28] $KNaAe_2H_6$ (Ae = Be, Mg, Ca),[29] K_2LiGaH_6,[30] and Mg_3XH_8 (X = Ca, Sc, Ti, V, Cr, Mn)[31] have been explored. These studies have demonstrated the importance of electronic structure and lattice interactions in determining hydrogen storage performance. For this purpose, transition metal hydrides such as alkali-alkaline-earth $KSrIrH_6$ and $KSrRhH_6$ represent very promising systems due to their constrained ligand-bonding environment, which can be tailored to maximize both hydrogen affinity and mechanical stability. Transition metal substitution with iridium (Ir) or rhodium (Rh) improves the metal-hydrogen bonding strengths and then better storage properties, and at the same time, increases the lattice mechanical stability through high cohesive energies. The $KSrIrH_6$ and $KSrRhH_6$ share a common crystal structure in which $[M(III)H_6]^{3-}$ (M = Ir, Rh) octahedral units are supported by alkali and alkaline earth cations (K^+ and Sr^{2+}),[32] forming an ionic framework that plays a crucial role in modulating the electronic structure and stability of the hydrides. Despite their favorable properties, systematic studies of the physical properties of $KSrIrH_6$ and $KSrRhH_6$, i.e., their structural, electronic, mechanical, optical, dynamical, and thermodynamic characteristics, remain limited. Here, we apply first-principles calculations to systematically investigate these properties and assess the hydrogen storage capability of $KSrIrH_6$ and $KSrRhH_6$.

2. Computational Analysis

Density functional theory (DFT) based first-principles calculations were carried out using the Quantum ESPRESSO (QE) package,[33] employing the projector augmented wave (PAW) method. Computations in QE were carried out using ultrasoft pseudopotentials sourced from the Garrity–Bennett–Rabe–Vanderbilt (GBRV) library.[34] The Perdew–Burke–Ernzerhof, generalized gradient approximation (PBE-GGA)[35,36] was used to determine the exchange correlation energy. Structural optimization was performed using the Broyden–Fletcher–Goldfarb–Shanno (BFGS) quasi-Newton algorithm,[37] which minimized both atomic forces and stress components. The wave function cutoff was set to 70 Ry, the charge density to 700 Ry, and SCF computations had a convergence threshold of 10^{-8} Ry. The phonon band structure was calculated using primitive unit cells containing nine atoms, employing the thermo_pw package[38] integrated with QE. The computational parameters were kept consistent with those used during the structural optimization of all hydrides. The thermo_pw algorithm was also used to calculate elastic constants (C_{ij}), and the associated mechanical properties using the energy-strain approach. Furthermore, the thermodynamic properties are explored using quantum quasi-harmonic approximation. In addition, ab initio molecular dynamics (AIMD) simulations based on the QE package in the NVT ensemble were performed at a time step of 1 fs for a total simulation time of 5 ps to assess the system's thermal stability.

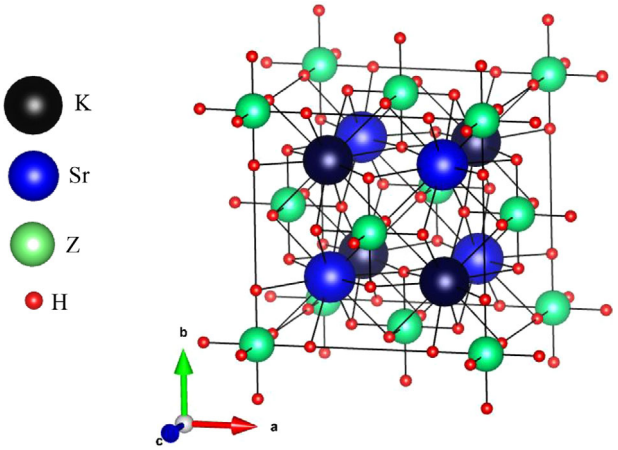

Figure 1. 3D schematic visualization of the unit cell of $KSrZH_6$ (Z = Rh, Ir) hydrides.

Table 1. The optimized lattice parameters and H_2 storage capacity of $KSrZH_6$ (Z = Rh, Ir).

Materials	A [Å]	V [Å^3]	B [GPa]	B′	E_0 [eV]	$C_{wt.\%}$
$KSrRhH_6$	7.79	118.16	33.01	4.41	−4161.17	2.57
$KSrIrH_6$	7.80	118.58	34.20	4.70	−4300.38	1.86

3. Results and Discussion

3.1. Structural and Hydrogen Storage Properties

The $KSrZH_6$ (Z = Rh, Ir) compounds crystallize in the cubic crystal structure with $F\bar{4}3m$ (No. 216) space group. The optimized crystal structure of $KSrZH_6$ (Z = Rh, Ir) hydrides is represented in **Figure 1**. Before analyzing a material's broader physical properties, it is critical to calculate its structural properties first. As shown in **Figure 2**a,b, the equilibrium lattice parameters were determined by optimizing the total energy of $KSrRhH_6$ and $KSrIrH_6$ compounds based on unit cell volume using fitting the computed data with the Birch–Murnaghan equation of state, given as[39,40]:

$$E(V) = E_0(V) + \frac{BV}{B'}\left[\frac{\left(\frac{V_0}{V}\right)^{B'}}{B'-1} + 1\right] - \frac{BV_0}{B'-1} \quad (1)$$

Moreover, **Table 1** gives an overview of the structural parameters of $KSrRhH_6$ and $KSrIrH_6$, including the optimized lattice parameter (a), the unit cell volume (V), the bulk modulus (B), the pressure derivative of the bulk modulus (B′), the minimum energy (E_n) and the gravimetric hydrogen storage capacity ($C_{wt.\%}$).

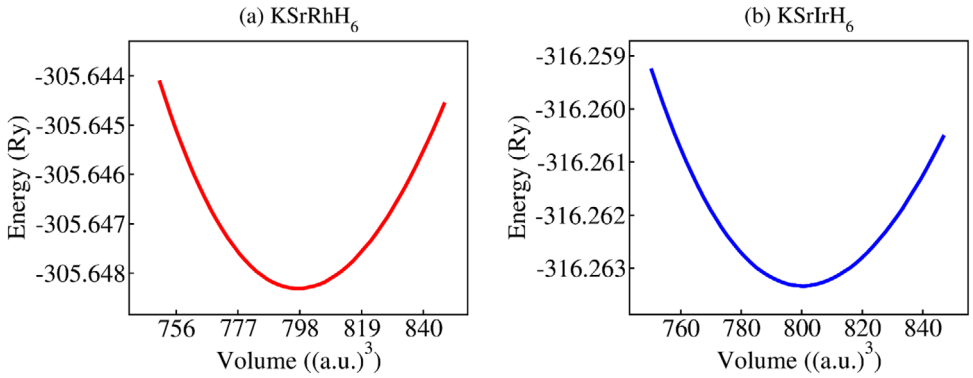

Figure 2. The optimized energy-volume plots of $KSrZH_6$ (Z = Rh, Ir).

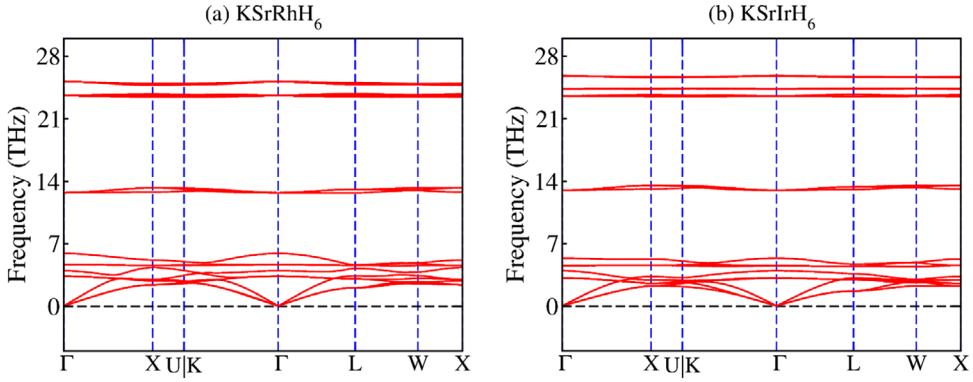

Figure 3. Phonon band diagram for a) $KSrRhH_6$, and b) $KSrIrH_6$.

The results show that $KSrIrH_6$ has a slightly higher lattice constant (a = 7.80 Å) than $KSrRhH_6$ (a = 7.79 Å). Furthermore, $KSrIrH_6$ has a subtly higher value of B (34.20 GPa) and B′ (4.70) than $KSrRhH_6$ (B = 33.01 GPa and B′ = 4.41), indicating that the Ir-based hydride is less compressible. Table 1 shows that the negative total minimum energies confirm the thermodynamic stability of the two hydrides,[39,40] which can be easily and fast prepared in experiments. The gravimetric hydrogen storage capacity ($C_{wt.\%}$) of $KSrZH_6$ with Z = Ir and Rh, is obtained utilizing the following equation[41]:

$$C_{wt\%} = \left(\frac{\left(\frac{H}{M}\right) m_H}{m_{Host} + \left(\frac{H}{M}\right) m_H} \times 100 \right) \% \quad (2)$$

where m_H and m_{Host} refer to the molar masses of hydrogen and host, respectively. (H/M) represents the number of hydrogen atoms to the number of compound atoms. Table 1 reveals that the $KSrRhH_6$ compound exhibits a higher hydrogen storage capacity (2.57 wt.%) compared to $KSrIrH_6$, which stores 1.86 wt.%. This can be explained by the difference in the atomic masses of Rh and Ir, which have a direct impact on the hydrogen-to-host mass ratio. Moreover, the hydrogen storage capacity of $KSrRhH_6$ surpasses that of several previously reported materials, such as Cs_2CaCdH_6 (1.39 wt.%),[42] Cs_2CaTlH_6 (1.78 wt.%),[24] and Cs_2BaTlH_6 (1.53 wt.%).[24]

3.2. Phonon and AIMD Calculation

The dynamical stability of the complex hydrides $KSrZH_6$ (Z = Ir, Rh) has been calculated by using the phonon dispersion analysis, as illustrated in **Figure** 3a,b. The phonon dispersion curves reveal two different types of vibrational modes: the optical branches in the higher frequency range (≈14–28 THz) result from out-of-phase vibrations of the atoms and are responsible for the optical properties of these hydrides, while the acoustic branches at low frequencies (≈0–7 THz) result from coordinated atomic vibrations and determine the elastic response of the material. According to theoretical principles, a dynamically stable structure should have only positive vibrational states,[43] since negative frequencies imply a loss of crystal binding energy, which leads to structural failure. Therefore, the absence of imaginary phonon modes suggests that $KSrRhH_6$ and $KSrIrH_6$ are structurally stable and thermodynamically viable compounds. To evaluate the thermal stability of $KSrZH_6$ (Z = Ir, Rh), we conducted ab initio molecular dynamics (AIMD) simulations at 300 K, with a total simulation time of 5 ps and a time step of 1 fs, using the Andersen thermostat within the NVT ensemble. As shown in **Figure** 4a,b, the results demonstrate energy variations of less than 0.03 Ry per atom, indicating minimal energy drift. Since thermodynamically stable materials maintain nearly constant total energy in AIMD simulations, confirming the structural integrity and robustness of $KSrRhH_6$ and $KSrIrH_6$ at room temperature conditions. This stability demonstrates their promise for practical use in hydride-

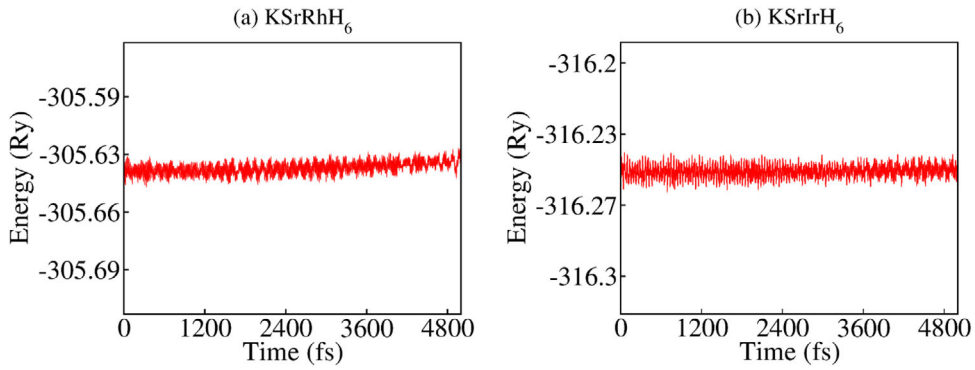

Figure 4. The total energy variation at 300 K assessed through AIMD simulations of $KSrZH_6$ (Z = Rh, Ir) hydrides.

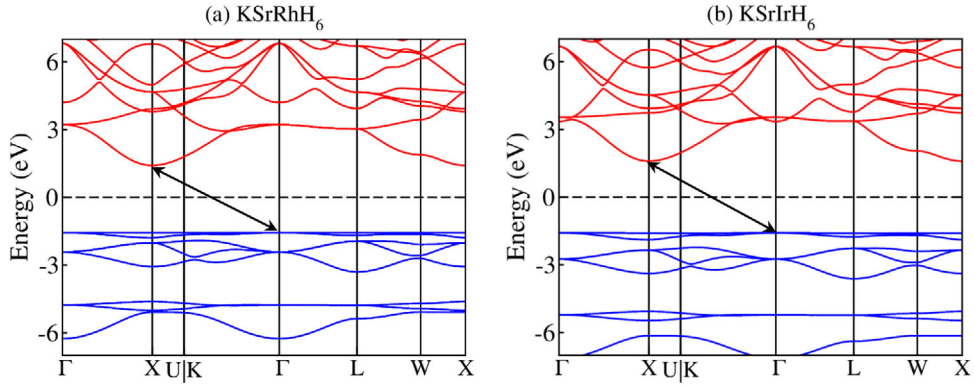

Figure 5. The electronic band structure for $KSrZH_6$ (Z = Rh, Ir) with the PBE-GGA method.

based materials and indicates that they can be synthesized using the direct combination method reported in Ref. [32].

3.3. Electronic Properties

The electronic properties of $KSrZH_6$ (Z = Ir, Rh) compounds are explored using the PBE-GGA approximation. **Figure** 5a,b depicts the electronic band structure of $KSrIrH_6$ and $KSrRhH_6$ in the energy range [−7–7 eV]. As observed in Figure 5, both compounds exhibit an indirect bandgap, since VBM and CBM are located in different k-points in the Brillouin zone, indicating an indirect electronic transition. The bandgap values were determined to be 2.97 and 3.17 eV for $KSrRhH_6$ and $KSrIrH_6$, respectively. Moreover, **Figure** 6a,b shows the total and partial densities of states (PDOS), which include the contributions of various atomic orbitals, and show the electronic structures of $KSrRhH_6$ and $KSrIrH_6$. It is clear that the d-orbitals (Rh-d and Ir-d) of the transition metal are most prominent in the region around the Fermi level (0 eV), indicating that they contribute to the electronic properties of the compounds. While the hydrogen s-orbitals show significant contributions at lower energies, suggesting a strong hybridization with Sr and Rh/Ir orbitals. Besides, the total density of states shows the distribution of electronic states in energy levels, with differences between the two compounds suggesting electronic conductivity or band structure differences. The higher delocalization of Ir-d states in $KSrIrH_6$ compared to Rh-d in $KSrRhH_6$ indicates that the Ir substitution may affect bonding strength and electronic behavior.

3.4. Optical Properties

A material's behavior is largely determined by its optical characteristics.[44] Correlating these features and computing them using Maxwell's equations can lead to a better knowledge and precise prediction of a material's optical response under various conditions. One of the most crucial characteristics for exploring a material's optical response is the dielectric function, $\varepsilon(\omega)$, which has two parts: the imaginary portion, $\varepsilon_2(\omega)$, which represents absorption, and the real portion, $\varepsilon_1(\omega)$, which represents dispersion.[45,46]

$$\varepsilon(\omega) = \varepsilon_1(\omega) + i\varepsilon_2(\omega) \tag{3}$$

For photon absorption resulting from electronic transitions and with excitation probability to the conduction band from the valence band, the imaginary component, $\varepsilon_2(\omega)$, is of the greatest interest. The material's polarizability and dispersive behavior in the presence of an applied external electric field and electromagnetic radiation interaction are determined by the real component, $\varepsilon_1(\omega)$. Moreover, Kramers–Kronig relations, one of the basic connections between real and imaginary dielectric functions, can be

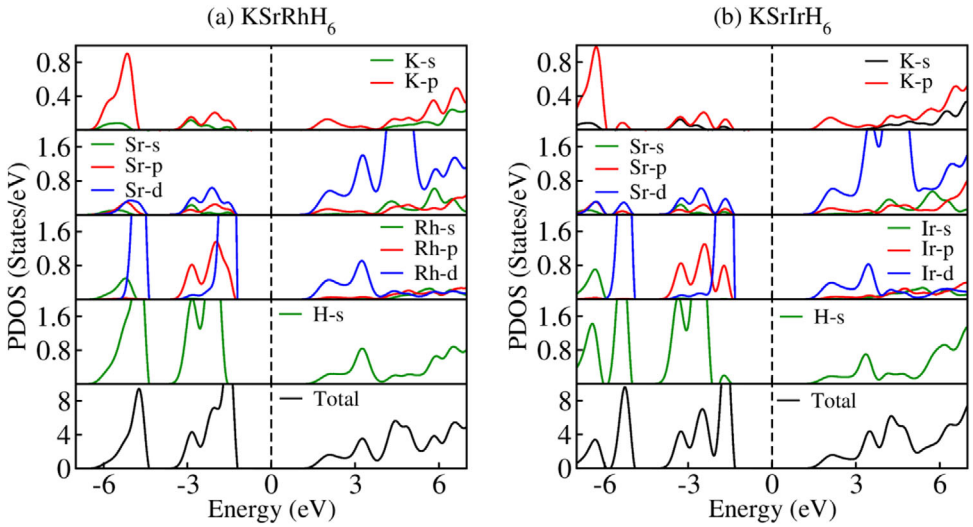

Figure 6. Computed density of states (DOS) of $KSrZH_6$ (Z = Rh, Ir).

used to derive $\varepsilon_1(\omega)$ from $\varepsilon_2(\omega)$.[47,48]

$$\varepsilon_2(\omega) = \frac{(4\pi^2 e^2)}{(\pi\omega^2 m^2)} \sum_{ij} \int_{BZ}^{\infty} [M_{ij}(k)]^2 f_i(1 - f_j)\, \delta[E_f - E_i - \omega] d^3k \tag{4}$$

$$\varepsilon_1(\omega) = 1 + \frac{2}{\pi} P \int_0^{\infty} \frac{\omega' \varepsilon_2(\omega')}{\omega'^2 - \omega^2} d\omega' \tag{5}$$

where the electron's mass and charge are denoted by m and e, respectively. The P indicates the matrix components of the valence to conduction band transitions. Additionally, f_i and E_i stand for the electron energy in the i-th state and the Fermi–Dirac distribution, respectively. Various optical properties, i.e., absorption coefficient $\alpha(\omega)$, reflectivity $R(\omega)$, refractive index $n(\omega)$, and extinction coefficient $k(\omega)$, can be described with the help of the following equations[49–53]:

$$\alpha(\omega) = \sqrt{2\omega} \left[-\varepsilon_1(\omega) + \sqrt{\varepsilon_1^2(\omega) + \varepsilon_2^2(\omega)} \right]^{1/2} \tag{6}$$

$$R(\omega) = \left| \frac{\sqrt{\varepsilon(\omega)} - 1}{\sqrt{\varepsilon(\omega)} + 1} \right|^2 \tag{7}$$

$$n(\omega) = \left[\frac{\sqrt{\varepsilon_1^2(\omega) + \varepsilon_2^2(\omega)} + \varepsilon_1(\omega)}{2} \right]^{1/2} \tag{8}$$

$$k(\omega) = \left[\frac{\sqrt{\varepsilon_1^2(\omega) + \varepsilon_2^2(\omega)} - \varepsilon_1(\omega)}{2} \right]^{1/2} \tag{9}$$

The real and imaginary parts of $\varepsilon(\omega)$ are calculated and listed in **Figure** 7a,b. The $\varepsilon_1(\omega)$, which determines the refractive index and polarization response,[54] exhibits a high peak between 3–6 eV, followed by a slow decline at higher energies. This suggests a substantial dielectric response through the lower energy range, with $KSrIrH_6$ showing minute shifts compared to $KSrRhH_6$, demonstrating that the Ir substitution alters the electronic environment and optical dispersion. At the same time, the $\varepsilon_2(\omega)$, which corresponds to optical absorption from electronic transitions, exhibits a prominent peak in the 5–7 eV range, indicating strong interband transitions. Most importantly, $KSrIrH_6$ shows slightly higher light absorption than $KSrRhH_6$, indicating that the inclusion of Ir increases electronic excitations and alters matter-light interactions. Furthermore, with increasing photon energy, both compounds exhibit gradually decreasing absorption, indicating a reduced density of available electronic states for the transitions.

Besides, **Figure** 8a presents the calculated absorption spectra of $KSrZH_6$ (Z = Rh, Ir) compounds. It is found that the absorption coefficient rises significantly at high photon energies, with well-defined peaks in the UV region. The $KSrIrH_6$ material shows a larger absorption magnitude than $KSrRhH_6$, indicating more intense light-matter interactions for the Ir compound. The sharp rise in absorption at ≈3 eV suggests the intense onset of optical transitions, which is important for the determination of the bandgap energy. The high UV absorption suggests applications in UV photodetectors, solar cells, and optical coatings. The optical absorption behavior also provides insight into the stability of the material under irradiation, a consideration of paramount importance for solar hydrogen storage materials. Moreover, the reflectivity spectra, which are shown in Figure 8b shows a moderate reflectance at lower photon energies with multiple peaks at higher energies. The reflectivity is below 0.3 over the energy range considered, indicating that these materials have low reflectance and high transmittance. While the peaks in the feature indicate the presence of electronic transitions and strong interband interactions. The $KSrIrH_6$ material is slightly more reflective than $KSrRhH_6$ overall, reflecting differences in surface optical response and electronic band structure. For hydrogen storage

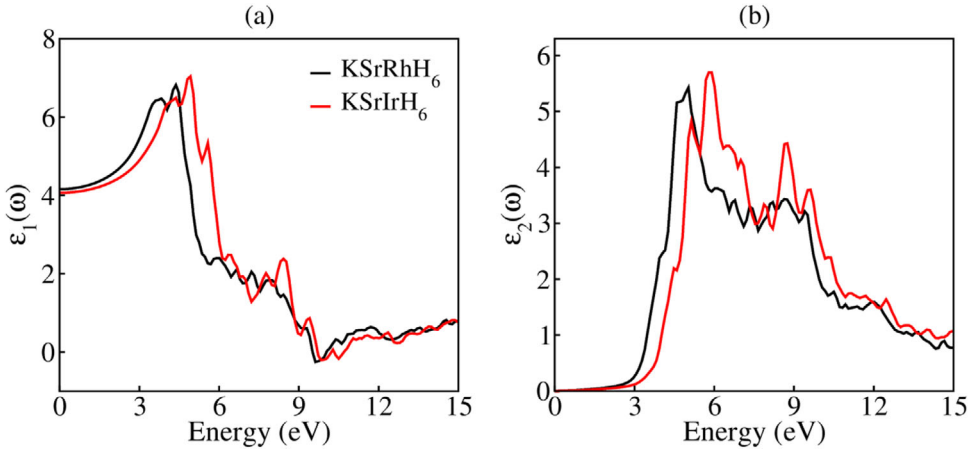

Figure 7. Calculated spectra of (a,b) dielectric function (real & imaginary part) of $KSrZH_6$ (Z = Rh, Ir) against photon energy.

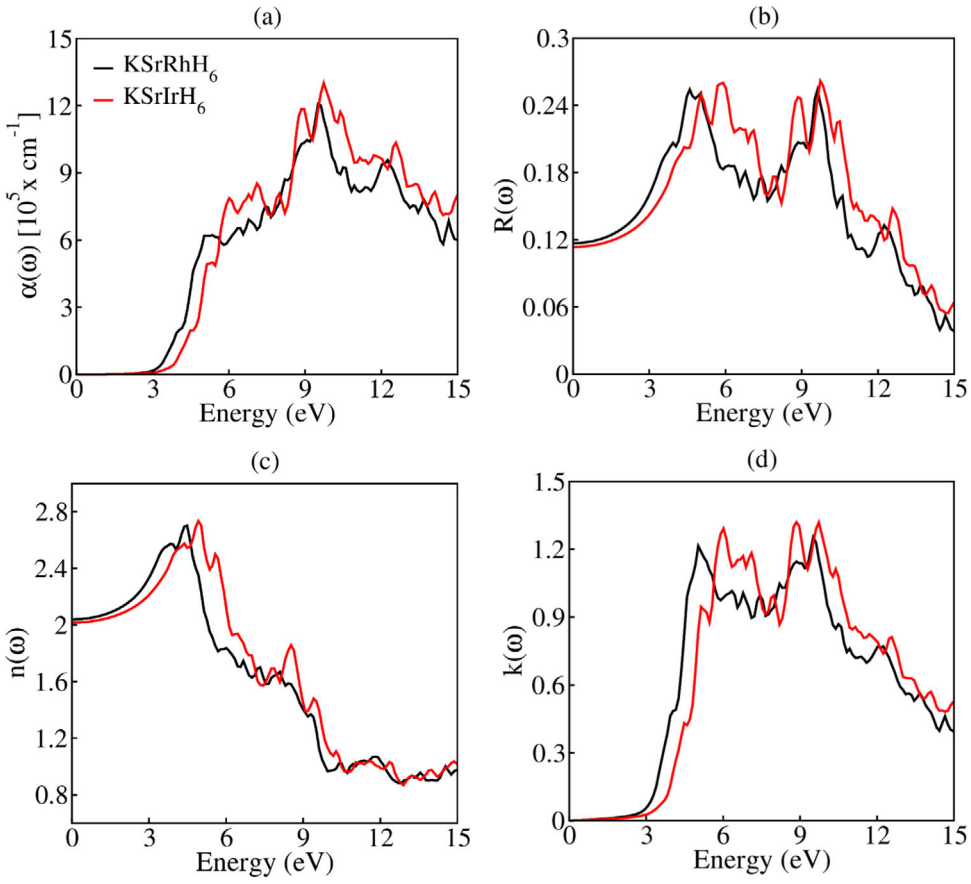

Figure 8. Calculated spectra of a) absorption, b) reflectivity, c) refractive index, and d) extinction coefficient of $KSrZH_6$ (Z = Rh, Ir) against photon energy.

applications, the low reflectivity value is preferable as it represents energy loss during the hydrogen adsorption and desorption processes when exposed to light. Figure 8c presents the refractive index variations, which shows a peak at lower photon energies with lower values at higher energies. The peak value of the refractive index occurs near the band-edge transition region, indicating a high dispersion of the light. Furthermore, high refractive index values for $KSrIrH_6$ compared to $KSrRhH_6$ indicate its greater potential to slow light propagation, a desirable property for photonic devices and optical waveguide applications. In hydrogen storage applications, the refractive index provides a sense of material transparency and interaction with electromagnetic radiation, which can influence the kinetics of hydrogen release under optical stimulation.

Table 2. Elastic constant (C_{ij}, GPa) of $KSrZH_6$ (Z = Rh, Ir).

Materials	C_{11}	C_{12}	C_{44}
$KSrRhH_6$	66.72	16.86	23.89
$KSrIrH_6$	64.76	18.16	24.60

Table 3. Mechanical attributes of $KSrZH_6$ (Z = Rh, Ir).

Materials	B	G	E	$C_p = C_{12}-C_{44}$	ν	B/G	A
$KSrRhH_6$	33.48	24.30	58.70	−7.03	0.21	1.38	0.96
$KSrIrH_6$	33.70	24.07	58.32	−6.44	0.21	1.40	1.06

The significant electronic transitions, as revealed in Figure 8d, are indicated in the UV region, where the extinction coefficient is highest. Greater light attenuation in the material is indicated by greater extinction coefficient values of $KSrIrH_6$ than $KSrRhH_6$. This attribute is directly proportional to the material's absorption behavior, this characteristic is especially relevant when researching optical losses for device applications like optoelectronic modulators and photodetectors. The higher extinction coefficients would suggest strong photon interactions in hydrogen storage, which would improve the kinetics of hydrogen desorption photo thermally. In general, the optical spectra demonstrate that both compounds exhibit high absorption, medium reflection, and large dispersion in the UV range. The greater absorption and extinction coefficient values of $KSrIrH_6$ suggest that it may have a more favorable optoelectronic performance than $KSrRhH_6$. These optical characteristics also imply that $KSrZH_6$ compounds might be great options for hydrogen storage applications that take into account light-induced desorption mechanisms.

3.5. Elastic and Mechanical Properties

The complex hydride compounds $KSrZH_6$ (Z = Ir and Rh), have various mechanical properties that influence their stability and potential applications. The hardness of a material, or its resistance to deformation when pushed, is crucial in determining the structural strength of $KSrZH_6$ (Z = Ir and Rh). The calculated elastic constants are shown in **Table 2**, and are checked for elastic stability using Born–Huang criterion[55]:

$$C_{11} > 0, C_{11} - C_{12} > 0, C_{11} + 2C_{12} > 0, C_{11} > B_0 > C_{12} \quad (10)$$

The mechanical stability of the $KSrZH_6$ (Z = Ir and Rh) materials under study is confirmed by their satisfaction of the aforementioned requirements. The Voigt, Reuss, and Hill approximation methods were used to compute the bulk modulus (B), shear modulus (G), and Young's modulus (E) in order to comprehend the mechanical properties of $KSrZH_6$ (Z = Ir and Rh).[56] The mechanical characteristics of $KSrZH_6$ (Z = Ir and Rh) are displayed in **Table 3**. When evaluating the stiffness of a material, Young's modulus (E) is a crucial quantity.[57] The stiffness differences between $KSrIrH_6$ and $KSrRhH_6$ are shown in Table 3's E values, which also shed light on their mechanical characteristics and potential uses. $KSrIrH_6$ and $KSrRhH_6$ have the same resistance to uniform compression, as indicated by their respective bulk modulus (B) of 33.48 GPa and 33.70 GPa. The two compounds, $KSrRhH_6$ at 24.30 GPa and $KSrIrH_6$ at 24.07 GPa, also have almost similar shear moduli-indicating comparable resistance to shape deformation under shear stress.[58] Young's modulus (E), the measure of material stiffness, is very similar to $KSrRhH_6$, slightly higher at 58.70 GPa compared to $KSrIrH_6$ at 58.32 GPa. The positive or negative value of Cauchy pressure (C_p) indicates the ductility or brittleness of a compound, respectively.[59] The calculated negative values of C_p indicate the brittleness of the studied materials. Poisson's ratio (ν), which describes the lateral deformation under compression, is the same for both compounds at 0.21, indicating similar deformation behavior under stress. The Pugh's index (B/G) for both materials is below the ductility criterion of 1.75 at 1.38 for $KSrRhH_6$ and 1.40 for $KSrIrH_6$, again supporting that the two materials are brittle. Finally, the anisotropy factor (*A*) is slightly different between the two materials. $KSrIrH_6$ has a value of 1.06 for *A*, showing a higher degree of anisotropy than $KSrRhH_6$ with *A* of 0.96. Overall, the mechanical study of $KSrRhH_6$ and $KSrIrH_6$ proves that the two compounds have similar mechanical behavior, with $KSrRhH_6$ being slightly stiffer and $KSrIrH_6$ having a slightly higher degree of anisotropy. Both compounds are classified as brittle based on their Cauchy pressure, Poisson's ratio, and Pugh's ratio parameters.

3.6. Thermodynamic Properties

The thermodynamic properties of $KSrZH_6$ (Z = Rh, Ir) as a function of temperature are shown in **Figure 9**a,b, which shows the change in entropy (E), heat capacity (C_v), energy (S), and free energy (F). All of these properties provide a better understanding of the thermal properties and thermal stability of the compounds. Starting with entropy, both $KSrRhH_6$ and $KSrIrH_6$ increase with increasing temperature, reflecting the greater disorder in the system with greater thermal vibrations. As the temperature increases, the lattice vibrations become more energetic, leading to greater excitation of the electrons and an increase in entropy. Surprisingly, $KSrRhH_6$ has a slightly higher entropy than $KSrIrH_6$, reflecting the greater disorder in the former compound at elevated temperatures. The heat capacity also increases with temperature for both materials, a typical trend following the Dulong–Petit law at high temperatures. $KSrRhH_6$ and $KSrIrH_6$ both stabilise at a constant value of ≈200 J K^{-1} mol^{-1} at high temperatures, indicating that the vibrational properties of both materials are similar and stabilise at this value with minimal difference between the two materials. The variation in energy numerically increases almost linearly with temperature for $KSrRhH_6$ and $KSrIrH_6$ to ≈200 kJ mol^{-1} at 800 K. This means that the materials respond similarly to thermal energy and both materials exhibit very similar vibrational contributions with increasing temperature. Finally, the free energy is also lower at higher temperatures, as would be the case for most materials. $KSrRhH_6$ is in the region of −150 kJ mol^{-1} at 800 K, but $KSrIrH_6$ is slightly lower at −180 kJ mol^{-1}, and therefore $KSrIrH_6$ is thermodynamically more stable at higher temperatures. In summary, while both $KSrRhH_6$ and $KSrIrH_6$ exhibit similar thermal behaviour, $KSrRhH_6$ exhibits slightly higher entropy, reflecting greater disorder at elevated temperatures, while $KSrIrH_6$ exhibits slightly

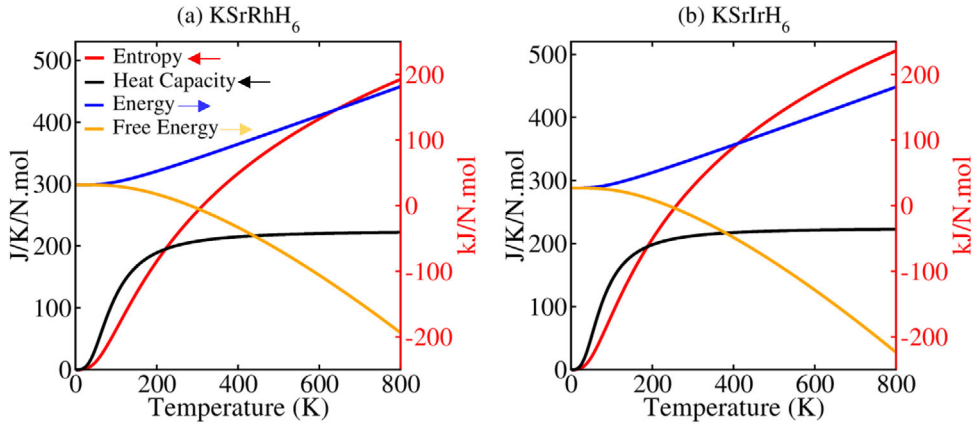

Figure 9. The variation in entropy, heat capacity, energy, and free energy against the temperature of (a) $KSrRhH_6$, and (b) $KSrIrH_6$.

greater stability in terms of free energy. These thermodynamic properties confirm that both materials are well suited to high temperature applications, with $KSrIrH_6$ having a slight advantage in thermodynamic stability.

4. Conclusion

This study comprehensively investigates the physical properties and hydrogen storage capability of $KSrZH_6$ (Z = Rh, Ir) complex hydrides using DFT to assess their potential for hydrogen storage and related applications. Structural analysis indicates that these materials form stable cubic structures, with lattice constants of 7.79 Å for $KSrRhH_6$ and 7.80 Å for $KSrIrH_6$, respectively. Phonon dispersion calculation confirms their dynamic stability. Furthermore, an extensive AIMD simulation evaluation verifies the absolute stability of all examined compounds, as evidenced by negligible variations in equilibrium energy, dispelling any doubts about structural dependability for practical applications. Both hydrides exhibit indirect semiconducting behavior with strong hybridization of H-1s and Rh/Ir-d states. The materials show good UV absorption and adequate optical properties and making them suitable for use in optoelectronic devices. The mechanical analysis confirms stability, brittleness, and anisotropic nature, while the thermodynamic assessment reveals consistent stability across a broad temperature range. In terms of hydrogen storage, $KSrRhH_6$ demonstrated a superior gravimetric capacity of 2.57 wt.%, highlighting its potential for efficient hydrogen storage applications, whereas $KSrIrH_6$ exhibited a capacity of 1.86 wt.%. In conclusion, this research provides valuable understanding of the suitability of $KSrRhH_6$ and $KSrIrH_6$ for sustainable energy technologies, opening avenues for future experimental confirmation and possible commercial implementation.

Acknowledgements

The authors extend their appreciation to the Deanship of Scientific Research and graduate studies at King Khalid University for funding this work through Large Groups Project under grant number (project number RGP.2/19/46. Academic year 1446H.

Conflict of Interest

The authors declare no conflict of interest.

Data Availability Statement

The data that support the findings of this study are available from the corresponding author upon reasonable request.

Keywords

AIMD, DFT, hydrogen storage, mechanical properties, phonon stability

Received: April 3, 2025
Revised: May 8, 2025
Published online:

[1] I. Dincer, C. Acar, *Int. J. Energy Res.* **2015**, *39*, 585.
[2] N. Abas, A. Kalair, N. Khan, *Futures* **2015**, *69*, 31.
[3] C. Withagen, *Resour. Energy Econ.* **1994**, *16*, 235.
[4] S. R. Chia, S. Nomanbhay, M. Y. Ong, A. H. Bin Shamsuddin, K. W. Chew, P. L. Show, *Fuel* **2022**, *314*, 123137.
[5] A. Midilli, M. Ay, I. Dincer, M. A. Rosen, *Renew. Sustain. Energy Rev.* **2005**, *9*, 255.
[6] Y. H. Teoh, H. G. How, T. D. Le, H. T. Nguyen, D. L. Loo, T. Rashid, F. Sher, *Fuel* **2023**, *333*, 126525.
[7] Y. Huang, C.-F. Yan, C.-Q. Guo, Z.-X. Lu, Y. Shi, Z.-D. Wang, *Int. J. Hydrogen Energy* **2017**, *42*, 4007.
[8] L. Zhang, C. Jia, F. Bai, W. Wang, S. An, K. Zhao, Z. Li, J. Li, H. Sun, *Fuel* **2024**, *355*, 129455.
[9] F. Zhang, P. Zhao, M. Niu, J. Maddy, *Int. J. Hydrogen Energy* **2016**, *41*, 14535.
[10] W. Sun, X. Kuang, H. D. J. Keen, C. Lu, A. Hermann, *Phys. Rev. B* **2020**, *102*, 144524.
[11] S. Niaz, T. Manzoor, A. H. Pandith, *Renew. Sustain. Energy Rev.* **2015**, *50*, 457.
[12] W. Sukmas, P. Tsuppayakorn-aek, P. Pluengphon, S. J. Clark, R. Ahuja, T. Bovornratanaraks, W. Luo, *Int. J. Hydrogen Energy* **2023**, *48*, 4006.
[13] P. Pluengphon, P. Tsuppayakorn-aek, W. Sukmas, B. Inceesungvorn, R. Ahuja, T. Bovornratanaraks, *Int. J. Hydrogen Energy* **2022**, *47*, 18763.
[14] P. Pluengphon, P. Tsuppayakorn-Aek, B. Inceesungvorn, R. Ahuja, T. Bovornratanaraks, *J. Phys. Chem. C* **2021**, *125*, 1723.

[15] T. Tang, Y. Tang, *Mater. Chem. Phys.* **2024**, *316*, 129099.
[16] T. Tang, Q. Dai, Q. Liang, Y. Wang, Z. Chen, Y. Tang, *Int. J. Hydrogen Energy* **2024**, *90*, 1333.
[17] S. Orimo, Y. Nakamori, J. R. Eliseo, A. Züttel, C. M. Jensen, *Chem. Rev.* **2007**, *107*, 4111.
[18] E. M. Dematteis, M. B. Amdisen, T. Autrey, J. Barale, M. E. Bowden, C. E. Buckley, Y. W. Cho, S. Deledda, M. Dornheim, P. De Jongh, *Prog. Energy* **2022**, *4*, 032009.
[19] J. Zhang, D. W. Zhou, P. Peng, J. S. Liu, *Physica B Condens. Matter* **2008**, *403*, 4217.
[20] J. Zhang, D. Zhou, J. Liu, *Trans. Nonferrous Met. Soc. China* **2009**, *19*, 205.
[21] H. Kim, S. Chi, S. Kang, B. C. Wood, M. Choi, E. S. Cho, *ACS Appl. Nano Mater.* **2025**, *8*, 4159.
[22] A. Hosen, D. Dahliah, N. F. A. Mohammad, A. A. Mousa, M. S. Abu-Jafar, *Int. J. Hydrogen Energy* **2025**, *102*, 348.
[23] A. Bouamrane, J. P. Laval, J.-P. Soulie, J. P. Bastide, *Mater. Res. Bull.* **2000**, *35*, 545.
[24] M. Shafqat Hayat, R. M. A. Khalil, *J. Mol. Graph. Model.* **2023**, *125*, 108600.
[25] H. Ammi, Z. Charifi, H. Baaziz, T. Ghellab, L. Bouhdjer, S. Adalla, H. Y. Ocak, Ş. Uğur, G. Uğur, *Int. J. Hydrogen Energy* **2024**, *87*, 966.
[26] Q. Dai, T.-Y. Tang, Q.-Q. Liang, Z.-Q. Chen, Y. Wang, Y.-L. Tang, *Int. J. Hydrogen Energy* **2024**, *92*, 769.
[27] M. A. Rehman, Z. U. Rehman, M. Usman, S. Y. Alomar, M. J. Khan, J. Fatima, *Int. J. Hydrogen Energy* **2024**, *84*, 447.
[28] T. Tang, Y. Tang, *J. Energy Storage* **2025**, *108*, 115102.
[29] T. Tang, Y. Tang, *Int. J. Hydrogen Energy* **2024**, *61*, 13.
[30] A. Hosen, A. A. Mousa, E. Nemati-Kande, A. N. Khan, M. S. Abu-Jafar, E. Benassi, E. A. Elghmaz, N. S. Abd EL-Gawaad, J. Asad, *Surf. Interfaces* **2025**, 106608.
[31] T. Tang, Y. Tang, *Int. J. Hydrogen Energy* **2024**, *74*, 372.
[32] K. Kadir, D. Moser, M. Munzel, D. Noreus, *Inorg. Chem.* **2011**, *50*, 11890.
[33] P. Giannozzi, S. Baroni, N. Bonini, M. Calandra, R. Car, C. Cavazzoni, D. Ceresoli, G. L. Chiarotti, M. Cococcioni, I. Dabo, *J. Phys.: Condens. Matter* **2009**, *21*, 395502.
[34] K. F. Garrity, J. W. Bennett, K. M. Rabe, D. Vanderbilt, *Comput. Mater. Sci.* **2014**, *81*, 446.
[35] J. P. Perdew, K. Burke, M. Ernzerhof, *Phys. Rev. Lett.* **1996**, *77*, 3865.
[36] J. P. Perdew, *Chem. Phys. Lett.* **1979**, *64*, 127.
[37] T. H. Fischer, J. Almlof, *J. Phys. Chem.* **1992**, *96*, 9768.
[38] X. Gong, A. Dal Corso, *Comput. Phys. Commun.* **2025**, *308*, 109439.
[39] F. D. Murnaghan, *Proc. Natl. Acad. Sci. USA* **1944**, *30*, 244.
[40] F. Birch, *Phys. Rev.* **1947**, *71*, 809.
[41] Y. Song, M. K. Shahzad, S. Hussain, A. Farrukh, M. Riaz, H. Sattar, G. Khan, G. A. Ashraf, S. M. Ali, M. Alam, *Int. J. Hydrogen Energy* **2024**, *79*, 1472.
[42] W. Azeem, S. Hussain, M. K. Shahzad, F. Azad, G. Khan, V. Tirth, H. Alqahtani, A. Algahtani, T. Al-Mughanam, Y. H. Wong, *Int. J. Hydrogen Energy* **2024**, *79*, 514.
[43] M. A. Hossain, A. Hosen, H. A. Abdulhussein, A. A. Mousa, M. M. Hasan, I. A. Ovi, M. R. Islam, R. K. Pingak, M. S. Abu-Jafar, *Results Eng.* **2024**, *24*, 103340.
[44] A. Hosen, *Heliyon* **2024**, *10*, 35855.
[45] B. Akenoun, S. Dahbi, H. Ez-Zahraouy, N. Tahiri, *Inorg. Chem. Commun.* **2024**, *170*, 113260.
[46] S. Dahbi, H. M. Ghaithan, M. Alkadi, A. A. A. Ahmed, S. M. H. Qaid, *Opt. Quantum Electron.* **2024**, *56*, 507.
[47] S. Dahbi, N. Tahiri, O. El Bounagui, H. Ez-Zahraouy, *Superlattices Microstruct.* **2021**, *160*, 107058.
[48] S. Dahbi, N. Tahiri, O. El Bounagui, H. Ez-Zahraouy, *Chem. Phys.* **2021**, *544*, 111105.
[49] Z. Jin, Y. Wu, S. Li, Q. Wu, S. Chen, Y. Chen, W. Zhang, C. Zhang, *Results Phys.* **2021**, *22*, 103860.
[50] S. Dahbi, N. Tahiri, O. El Bounagui, H. Ez-Zahraouy, *Mater. Sci. Semicond. Process* **2022**, *138*, 106271.
[51] G. Guo, F. Du, G. Guo, P. Li, *Chin. J. Phys.* **2025**, *93*, 564.
[52] G. Guo, Y. Zhou, G. Guo, Z. Xie, *Mater Today Chem.* **2024**, *35*, 101913.
[53] G. Guo, Y. Chen, L. Mao, P. Li, *Surf. Interfaces* **2024**, *55*, 105413.
[54] M. Hasan, A. Hossain, H. A. Abdulhussein, A. Al Shadi, B. Sorker, A. A. Al-Khafagi, R. K. Pingak, D. Dahliah, M. S. Abu-Jafar, A. Hosen, *Inorg. Chem. Commun.* **2025**, *171*, 113607.
[55] M. Born, K. Huang, *Dynamical Theory of Crystal Lattices*, Oxford University Press, Oxford, UK **1996**.
[56] R. Hill, *Proc. Phys. Soc. Sect. A* **1952**, *65*, 349.
[57] H. A. Abdulhussein, M. A. Hossain, A. Hosen, D. Dahliah, M. S. Abu-Jafar, A. Harbi, R. K. Pingak, M. Moutaabbid, I. A. Ovi, M. R. Islam, *Mater. Sci. Semicond. Process* **2025**, *187*, 109133.
[58] A. Hosen, M. R. Islam, S. H. Badhan, *Heliyon* **2024**, *10*, 27581.
[59] A. Hosen, M. R. Islam, A. A. Mousa, M. S. Abu-Jafar, *Results in Eng.* **2025**, *25*, 104016.